Radiation Physics and Chemistry 177 (2020) 109113

Contents lists available at ScienceDirect

Radiation Physics and Chemistry

journal homepage: www.elsevier.com/locate/radphyschem

Evaluation of fetal, medical and occupational exposure in ERCP procedures using Monte Carlo simulation and virtual anthropomorphic phantoms

William S. Santos[a], Lucas W.G. Souza[b,e], Lucio P. Neves[*,a,b], Ana P. Perini[a,b], Carla J. Santos[b], Walmir Belinato[c], Linda V.E. Caldas[d]

[a] Instituto de Física, Universidade Federal de Uberlândia, Av. João Naves de Ávila 2121, 38400902, Uberlândia, MG, Brazil
[b] Programa de Pós-Graduação Em Engenharia Biomédica, Faculdade de Engenharia Elétrica, Universidade Federal de Uberlândia, Uberlândia, MG, Brazil
[c] Departamento de Ensino, Instituto Federal de Educação, Ciência e Tecnologia da Bahia, Av. Amazonas 3150, 45030-220, Vitória da Conquista, BA, Brazil
[d] Instituto de Pesquisas Energéticas e Nucleares, Comissão Nacional de Energia Nuclear (IPEN-CNEN/SP), Av. Prof. Lineu Prestes 2242, 05508-000, São Paulo, SP, Brazil
[e] Instituto Maria Ranulfa Ltda, FATRA - Faculdade do Trabalho. Av. Paes Leme Osvaldo, 38408000, Uberlândia, MG, Brazil

ARTICLE INFO

Keywords:
Endoscopic retrograde cholangiopancreatography
Monte Carlo simulation
Virtual anthropomorphic phantoms
Pregnant patient
Conversion coefficients

ABSTRACT

In this study, computational modeling was applied to evaluate medical and occupational exposure, to ionizing radiation, during the Endoscopic Retrograde Cholangiopancreatography (ERCP) procedure of a pregnant woman in the second gestational trimester. The fetal dose evaluation and the construction of a photon fluence map inside the procedure room were also performed. The medical staff and patient were represented by virtual anthropomorphic phantoms. These phantoms were incorporated to the radiation transport code MCNPX (version 2.7.0). The photon beam was projected on the right lateral lower section of the liver of the patient, producing a FOV of 15×15 cm^2. The spectral influence was evaluated using tube voltages of 70 kVp and 80 kVp with a total filtration of 5 mmAl. The influence of the suspended shield, lead curtain and fetal shield were evaluated on the Conversion Coefficients for Equivalent Dose ($CC[H_T]$) and Effective Dose ($CC[E]$) for the medical staff and patient. The removal of the lead curtain and suspended shield was considered the most critical configuration to the medical staff. In this situation, an increase up to 633% in the $CC[H_T]_{eye\ lens}$ and 900% in $CC[E]$, for the medical staff, was reached. The $CC[E]_{Patient}$ ranged between 0.13 mSv/Gy.cm^2 (70 kVp with all protective devices) and 0.15 mSv/Gy.cm^2 (80 kVp without fetal shield) and the values obtained are in agreement with the literature. The $CC[H_T]_{fetus}$ oscillated between 2.2E-1 mSv/Gy.cm^2 (70 kV with fetal shield) and 2.7E-1 mSv/Gy.cm^2 (80 kV without fetal shield). The outcomes of this work are useful in the prior monitoring of the radiation doses and risks, and a reduction on these may be reached for the medical team and patient, which is a complicated arrangement in ERCP procedures.

1. Introduction

The endoscopic retrograde cholangiopancreatography (ERCP) is a diagnostic and therapeutic procedure utilized to diagnose and treat biliary and pancreatic duct diseases (Samara et al., 2009). By means of an endoscopic exam, a flexible tube is introduced through the patient mouth, passing through the oesophagus, stomach until the duodenum is reached. In this organ the major duodenal papilla is located, which enables the access to the liver and pancreatic ducts by means of a catheter inserted through the duodenoscope. This apparatus also allows the transport of contrast materials (iodine or barium) to the ducts enabling better visualization of the structures, if required by the physician. Despite the great benefits to the patient, since open surgical intervention is often avoided, it is important to highlight other risks involved, since in order to access the organ with suspected disease, or the local of treatment, the physician utilizes ionizing radiation to image the region (Al-Hashem et al., 2009). For pregnant patients, ERCP is commonly indicated to treat coledocolithiasis, which is the formation or presence of calculus inside the biliary ducts (Al-Hashem et al., 2009). When possible, the use of fluoroscopy can be replaced by ultrasound (US), magnetic resonance imaging (MRI) among other techniques (Wu et al., 2014).

The study performed by Samara et al. (2009) shows that 12% of the pregnant women population is affected by this type of disease and the complications increase with gestational age. Since fetal tissues are more sensitive to radiation, the doses involved in the pregnant patient must

* Corresponding author. Instituto de Física, Universidade Federal de Uberlândia, Av. João Naves de Ávila 2121, 38400902, Uberlândia, MG, Brazil.
E-mail addresses: william@ufu.br (W.S. Santos), lucasswill@ufu.br (L.W.G. Souza), lucio.neves@ufu.br (L.P. Neves), anapaula.perini@ufu.br (A.P. Perini), carlaafro@yahoo.com.br (C.J. Santos), wbfisica@gmail.com (W. Belinato), lcaldas@ipen.br (L.V.E. Caldas).

https://doi.org/10.1016/j.radphyschem.2020.109113
Received 7 February 2020; Received in revised form 25 June 2020; Accepted 15 July 2020
Available online 13 August 2020
0969-806X/

be carefully evaluated. Depending on the fetal dose and gestational phase, deterministic effects may arise, especially in the patient skin, as well as teratogenic effects (ICRP 103 (2007)). In the case of fetal doses above the 100 mGy threshold (ICRP 103, 2007), the pregnant patient has to receive enough information about the fetal dose magnitude and possible damages to the fetal development, as well as the cancer risks at adult age (ICRP 103, 2007).

There are only few data in the literature about evaluation of absorbed doses to pregnant patients, and the radiographic parameters that might affect the absorbed doses in these individuals. The published values for absorbed doses vary from 0.1 mGy to 3 mGy per procedure, and they may greatly diverge among studies, since the results were obtained for specific patients and radiographic techniques (Tham et al., 2003; Kahaleh et al., 2004).

In the literature the dosimetric results in ERCP, with the virtual anthropomorphic phantoms, were obtained just for the patients, while the effective dose for the medical staff were determined utilizing thermoluminescent dosimetry, whose results per procedure for main and assistant physicians were in the range of 14 μSv–4 μSv and 0.4 μSv–0.01 μSv, respectively (Sulieman et al., 2011). In another study performed with stylized phantoms, patient and fetus doses were evaluated for three gestational stages (Samara et al., 2009). However, it is important to highlight the low resemblance of stylized phantoms in respect to a real person, since the organ and other body structures are represented by geometric shapes described by mathematical equations (sphere, cone, ellipsoid, cylinder, etc) (Xu, 2014). Additionally, the organ/tissue distribution in the body, and the relative distance between organs and other structures, of that class of phantoms diverge from the reality and, therefore, more realistic virtual anthropomorphic phantoms must be used.

A remarkable feature of this work is that, beyond the fetus and patient dosimetric evaluation, occupational exposures were also investigated, since in ERCP procedures a close proximity between the main physician to both patient and X-ray tube is required. Since fluoroscopic and conventional radiographic images are required, and several parameters within these image modalities may lead to high absorbed doses to the patient and medical staff, a deep investigation of such procedures may provide important data to ensure better radiation protection policies. In this sense, it is necessary to establish a methodology to enable the estimative of doses with reliable techniques (Lee et al., 2019), thereby, allow a better evaluation of the effective (E) and equivalent (H_T) doses to all individuals exposed during an ERCP procedure. Unlike other studies that applied virtual anthropomorphic phantoms to represent only the patients, in this study, besides the patient, the irradiation scenario was composed, simultaneously, by a main and an assistant physicians.

The evaluation will be done utilizing conversion coefficients (CC) to estimate both equivalent and effective doses. The impacts of operational parameters change such as tube voltage, use or disuse of protective equipment such as lead curtain, fetal shield and suspended shield were evaluated. Besides that, the effectiveness of a fetus lead shield from the primary X-ray beam interception was also evaluated.

2. Materials and methods

2.1. Virtual anthropomorphic phantoms and the MCNPX Monte Carlo code

In this study, three virtual anthropomorphic phantoms, based on mesh surfaces, were utilized to represent a patient, in the second gestational trimester, and the physicians (male and female) involved in a ERCP procedure (Cassola et al., 2010; Kramer et al., 2009; Cabral et al., 2015). These phantoms are denominated MARIA (patient), MASH3 (male physician) and FASH3 (female physician). They were modeled by the *Computational Dosimetry Group* of the *Nuclear Energy Department* from the *Federal University of Pernambuco* (DEN/UFPE) (Cassola et al., 2010; Kramer et al., 2009; Cabral et al., 2015). The phantoms were developed based on the data for the reference male and female adult from IRCP 89 (ICRP 89, 2002). Some of the most important anthropomorphic features of each phantom are shown in Table 1 and an image of the three phantoms is presented in Fig. 1. These phantoms were coupled to the Monte Carlo N-Particle eXtended-MCNPX (2.7.0) code (Pelowitz, 2011), which is used to model the radiation transport and its possible interactions with materials. Therefore, the electron energy deposition on the materials enables the calculation of the absorbed doses in organs and tissues of the phantoms.

Table 1
Data of the adult virtual anthropomorphic phantoms: male (MASH3), female (FASH3) and pregnant patient (MARIA).

	Mass	Height	Matrix	BMI[a]	Voxel size
Phantom	(kg)	(cm)	(columns x lines x slices)	(kg/m^2)	(mm^3)
MASH3	73.0	176.0	239 × 129 x 731	23.6	
FASH3	60.0	163.0	221 × 128 x 677	22.7	2.4 × 2.4 x 2.4
MARIA	61.2	163.0	206 × 146 x 677	23.0	

[a] Body Mass Index.

Fig. 2 shows the geometric configuration of the main physician (Fig. 2 (D)), the assistant physician (Fig. 2 (N)), the patient position and the main equipment used during an ERCP procedure. The scenario was modeled with the MCNPX 2.7.0 code. Further information regarding the chemical and physical compositions of the materials used in this study is found in the work of Santos et al. (2018).

The main and assistant physicians were positioned in the patient left side at 33 and 105 cm distant from the patient waist, respectively (Fig. 2 (D) and (N)). In all scenarios, the medical staff utilized the personal protective equipment (PPE) such as lead eyewear (Fig. 2 (E)), thyroid shield (Fig. 2 (F)) and lead apron (Fig. 2 (M)). The collective protective equipment (CPE) lead curtain (Fig. 2 (A)) attached to the surgical table (Fig. 2 (I)), and suspended shield (Fig. 2 (C)), with a thickness equivalent to 0.5 mmPb, were also inserted in the simulations. The patient was considered sedated, and was placed in the lateral position on the table. We also added the fetal shield (Fig. 2 (B)) as a protective equipment designed to the fetus' protection. The fetal shield was positioned in the patient pelvic region (equivalent thickness of 0.5 mmPb). The table dimensions, which are comprised of a foam cushion above a carbon fiber base, are $60 \times 10 \times 200\ cm^3$, positioned 1 m above the room floor.

The right lateral (RLAT) beam projection was used in this work, with the beam covering a field size of $15 \times 15\ cm^2$ (Huda et al., 2015) at the center of the biliary bladder (medium plane) forming a field of view (FOV) of 30 cm diameter in the flat panel detector (Fig. 2 (H)) entrance.

The maximum photon energies utilized in the ERCP procedure were 70 keV and 80 keV and, therefore, the interaction processes considered most probable were the photoelectric absorption, with a fluorescent emission possibility and Auger electrons, coherent (Rayleigh) and incoherent (Compton) scattering. Photon and electron transport were calculated using the ENDF/B-VIII cross section library (Pelowitz, 2011). For all exposure scenarios, 1E9 photon histories were simulated, in order to assure low statistical uncertainties. Within this no variance reduction methods were employed.

Photon spectra were generated using the IPEM/SR78 (Cranley et al., 1997) software and incorporated to the MCNPX input file. The input parameters were peak tube voltages of 70 kVp and 80 kVp, 5 mmAl total filtration and anodic angle of 12° (Samara et al., 2009; Huda et al., 2015). The X-ray tube was modeled with a lead housing with a point photon source emitting a conical X-ray beam in its interior. The source solid angle was specified by the focal distance and the X-ray field dimensions, which covers the pregnant patient biliary bladder. The lead collimators were placed on the X-ray tube window to shape a rectangular FOV. The dose-area product (DAP) was calculated multiplying the air absorbed dose, which was obtained in an air cell with

Fig. 1. View of the male (MASH3), female (FASH3) and pregnant patient (MARIA) adult anthropomorphic phantoms (Cassola et al., 2010; Kramer et al., 2009; Cabral et al., 2015).

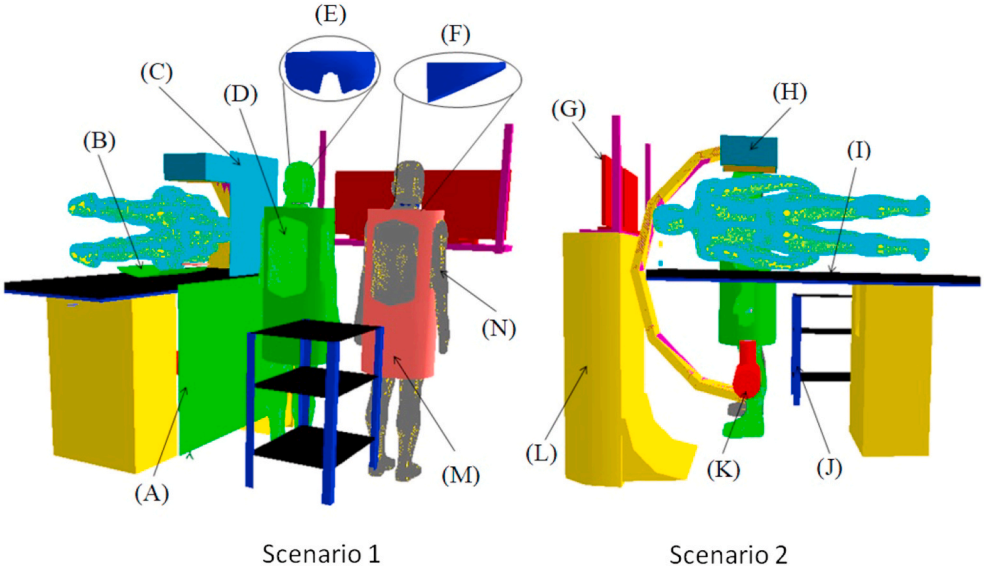

Fig. 2. Geometric configuration of the main equipment used in the Monte Carlo simulation: lead curtain (A), fetal shield (B), suspended shield (C), main physician (D), lead eyewear (E), thyroid shield (F), video monitors (G), flat panel detector (H), surgical table (I), surgical instrumentation table (J), X-ray tube (K), X-ray equipment (L), lead apron (M) and assistant physician (N). In scenario 1 all the protective equipment are presented, and in scenario 2 the lead curtain (A), fetal shield (B), suspended shield (C) were removed.

$4.6 \times 4.6 \times 1.0\ cm^3$, located at the X-ray tube exit and at 15 cm from the focus, by the beam area at this distance. The Monte Carlo uncertainty for the DAP was 0.01%.

2.2. Dosimetric calculation using the MCNPX code

The direct determination of the absorbed doses to the organs and tissues of the patient and medical staff is a difficult task, or even impossible, to be achieved in most cases. To overcome such difficulties, the Monte Carlo Method may be employed. Its accuracy as a dosimetric technique was recently studied in the work of Lee et al. (2019). They showed that the Monte Carlo simulation is comparable to termoluminescent dosimetric measurements in the effective dose determination, during pediatric panoramic radiography.

In this study, the dosimetric results are presented in the CC format, i.e., the fraction between the intended dosimetric protection quantity by another one, more easily measurable in the clinical practice, like the DAP. Therefore, the results of this work were normalized by this quantity, which is the $DAP_{simulated}$. In this way, the quantities $CC[H_T]$ and CC[E] refer to the conversion coefficients for equivalent and effective dose, respectively. Excepting the red bone marrow (RBM), the absorbed doses in the organs, tissues and other structures of the anthropomorphic phantoms were calculated using the tally *F6* (given in MeV/g/particle) of the MCNPX code. The multiplication of the mean photon fluence, calculated in each bone site, with the tally *F4* (MeV/cm^2/particle) by the result of the DE/DF dose function card was used to calculate the RBM dose. The CC[E] for the medical staff were calculated utilizing Equation (1) (ICRP 116, 2010).

$$CC[E] = \frac{CC[E]_{Male} + CC[E]_{Female}}{2} \quad (1)$$

where

$$CC[E]_{Male} = \sum_T w_T \times CC[H_T]_{Male} \quad (2)$$

$$CC[E]_{Female} = \sum_T w_T \times CC[H_T]_{Female} \quad (3)$$

$$CC[H_T] = \frac{MCNPX\ tally}{DAP_{simulated}} \quad (4)$$

where w_T is the tissue weighting factor, a value that represents the contribution of an organ or tissue to the overall stochastic risk from ionizing radiation exposure. These values are averaged for both genders and all ages (ICRP 103, 2007). The $CC[H_T]_{Male}$ and $CC[H_T]_{Female}$ are, respectively, the $CC[H_T]$ of the male and the female virtual anthropomorphic phantoms. The patient $CC[E]_{Patient}$ was calculated using Equation (5):

$$CC[E]_{Patient} = \sum_T w_T \times CC[H_T]_{Patient} \quad (5)$$

Along with the $CC[H_T]$ and CC[E] for patient and physicians, in this study, the cancer risk incidence for the fetus (R_{Fetus}) was evaluated as a result of the exposure to ionizing radiation during the ERCP procedure. It was calculated using Equation (6) (Brenner and Huda, 2008):

$$R_{Fetus} = \sum_T r_T \times CC[H_T]_{MCNPX\,(Fetus)} \times DAP_{Measured} \quad (6)$$

where r_T represents the cancer risk for each organ/tissue T. The cancer incidence risk coefficient to the fetus (soft tissue), due to a single exposure during the ERCP procedure, was collected from the literature (ICRP 103, 2007), which recommends a value of r_T = 5.5E-02 per Gy for cancer induction effect.

3. Results and discussion

The main results for the CC[E] and $CC[H_T]$ as a function of tube

Table 2
$CC[H_T]_{Male}$ and $CC[E]_{Male}$ (μSv/Gy.cm^2) for the male main and assistant physicians (MASH3): with lead curtain, suspended shield and fetal shield. Type A uncertainties are presented in parentheses (in %).

	Scenario with all protective equipment			
	70 kVp		80 kVp	
Male **Organ/ Tissue**	**Main Physician**	**Assistant Physician**	**Main Physician**	**Assistant Physician**
Bone marrow	6.4E-02 (0.3)	7.4E-03 (0.8)	1.0E-01 (0.2)	1.0E-02 (0.7)
Colon	2.6E-02 (2.2)	8.9E-04 (11)	4.9E-02 (1.6)	1.5E-03 (9.6)
Lung	8.1E-02 (0.8)	6.4E-03 (3.1)	1.5E-01 (0.6)	8.5E-03 (2.7)
Stomach	3.0E-02 (3.1)	6.8E-04 (21)	5.9E-02 (2.4)	7.4E-04 (22)
Breast	7.3E-02 (3.9)	2.6E-03 (23)	1.4E-01 (2.9)	3.0E-03 (25)
Remainder tissues[a]	7.6E-03 (0.2)	7.3E-04 (0.7)	1.2E-02 (0.2)	9.9E-04 (0.6)
Gonads	1.6E-03 (28)	1.4E-04 (66)	4.9E-03 (21)	2.1E-03 (35)
Bladder	1.7E-03 (19)	3.1E-04 (48)	3.5E-03 (12)	4.3E-04 (48)
Oesophagus	4.4E-02 (3.8)	5.4E-03 (14)	9.1E-02 (2.8)	7.2E-03 (12)
Liver	1.6E-01 (0.8)	2.7E-03 (6.1)	2.7E-01 (0.6)	3.8E-03 (5.5)
Thyroid	2.5E-02 (8.9)	6.8E-03 (19)	3.8E-02 (7.0)	8.1E-03 (17)
Bone surface	6.3E-02 (0.3)	2.0E-02 (0.8)	9.6E-02 (0.2)	2.7E-02 (0.7)
Brain	8.9E-02 (1.1)	1.6E-02 (2.8)	1.7E-01 (0.8)	2.3E-02 (2.4)
Salivary glands	3.2E-02 (2.1)	1.3E-02 (3.7)	5.4E-02 (1.6)	1.6E-02 (3.3)
Skin	1.7E-01 (0.2)	2.3E-02 (0.5)	2.4E-01 (0.2)	3.1E-02 (0.5)
Eye lens	8.4E-02 (12)	3.0E-02 (20)	1.7E-01 (9.0)	3.9E-02 (18)
$CC[E]_{Male}$ (μSv/Gy.cm^2)	4.7E-02 (2.0)	3.6E-03 (7.0)	8.4E-02 (2.0)	4.9E-03 (5.0)

[a] Adrenals, extratoracic region, gall bladder, kidneys, lymphatic nodes, muscle, oral mucosa, pancreas, prostate, small intestine, spleen, thymus and heart.

Table 3
$CC[H_T]_{Male}$ and $CC[E]_{Male}$ (μSv/Gy.cm^2) for the male main and assistant physicians (MASH3): without lead curtain and suspended shield. Type A uncertainties are presented in parentheses (*in* %).

	Scenario without lead curtain and suspended shield			
	70 kVp		80 kVp	
Male Organ/ Tissue	**Main Physician**	**Assistant Physician**	**Main Physician**	**Assistant Physician**
Bone marrow	6.2E-01 (0.1)	1.9E-02 (0.5)	7.8E-01 (0.1)	2.5E-02 (0.4)
Colon	2.4E-01 (0.7)	1.8E-03 (8.1)	3.3E-01 (0.6)	3.2E-03 (6.9)
Lung	8.0E-01 (0.3)	1.4E-02 (2.1)	1.1E+00 (0.2)	1.8E-02 (1.9)
Stomach	1.8E-01 (1.3)	1.7E-03 (16)	2.7E-01 (1.1)	1.7E-03 (15)
Breast	1.0E+00 (1.2)	8.4E-03 (14)	1.2E+00 (1.1)	1.0E-02 (14)
Remainder tissues[a]	7.0E-02 (0.1)	2.1E-03 (0.4)	8.5E-02 (0.1)	2.8E-03 (0.4)
Gonads	5.6E-02 (5.8)	1.2E-02 (12)	8.7E-02 (4.9)	2.2E-02 (9.5)
Bladder	1.4E-02 (6.6)	9.9E-04 (25)	2.3E-02 (5.5)	1.8E-03 (21)
Oesophagus	3.6E-01 (1.4)	8.5E-03 (12)	5.3E-01 (1.2)	1.2E-02 (8.8)
Liver	1.3E+00 (0.3)	5.2E-03 (4.4)	1.7E+00 (0.3)	7.1E-03 (3.9)
Thyroid	1.5E-01 (3.8)	1.3E-02 (15)	2.0E-01 (3.2)	1.5E-02 (12)
Bone surface	6.1E-01 (0.1)	5.0E-02 (0.5)	7.6E-01 (0.1)	6.7E-02 (0.5)
Brain	7.6E-01 (0.4)	3.4E-02 (1.9)	1.1E+00 (0.3)	4.9E-02 (1.7)
Salivary glands	2.8E-01 (0.7)	2.1E-02 (3.0)	3.6E-01 (0.6)	2.6E-02 (2.7)
Skin	1.9E+00 (0.1)	6.9E-02 (0.3)	2.1E+00 (0.1)	8.7E-02 (0.3)
Eye lens	6.2E-01 (5.0)	6.1E-02 (14)	8.2E-01 (4.0)	8.4E-02 (12)
$CC[E]_{Male}$ (μSv/Gy.cm^2)	4.6E-01 (1.0)	9.4E-03 (3.0)	6.0E-01 (1.0)	1.3E-02 (3.0)

[a] Adrenals, extratoracic region, gall bladder, kidneys, lymphatic nodes, muscle, oral mucosa, pancreas, prostate, small intestine, spleen, thymus and heart.

Table 4
$CC[H_T]_{Male}$ and $CC[E]_{Male}$ ($\mu Sv/Gy.cm^2$) for the male main and assistant physicians (MASH3): without fetal shield. Type A uncertainties are presented in parentheses (*in %*).

	Scenario without fetal shield			
	70 kVp		80 kVp	
Male **Organ/ Tissue**	**Main Physician**	**Assistant Physician**	**Main Physician**	**Assistant Physician**
Bone marrow	6.5E-02 (0.3)	8.1E-03 (0.8)	1.0E-01 (0.2)	1.1E-02 (0.7)
Colon	2.6E-02 (2.2)	1.0E-03 (11)	5.0E-02 (1.6)	1.8E-03 (8.8)
Lung	8.2E-02 (0.8)	7.1E-03 (2.9)	1.6E-01 (0.6)	9.4E-03 (2.6)
Stomach	3.1E-02 (3.1)	7.5E-04 (20)	6.0E-02 (2.3)	1.0E-03 (19)
Breast	7.3E-02 (3.9)	2.7E-03 (22)	1.4E-01 (2.9)	3.3E-03 (24)
Remainder tissues[a]	7.8E-03 (0.2)	8.1E-04 (0.6)	1.2E-02 (0.2)	1.1E-03 (0.6)
Gonads	1.7E-03 (27)	1.4E-04 (66)	5.0E-03 (20)	2.1E-03 (35)
Bladder	1.9E-03 (18)	3.1E-04 (48)	3.6E-03 (12)	5.6E-04 (40)
Oesophagus	4.5E-02 (3.8)	5.6E-03 (14)	9.2E-02 (2.8)	7.9E-03 (11)
Liver	1.6E-01 (0.8)	3.0E-03 (5.7)	2.7E-01 (0.6)	4.3E-03 (5.2)
Thyroid	2.5E-02 (8.9)	7.4E-03 (18)	3.9E-02 (7.0)	8.8E-03 (16)
Bone surface	6.4E-02 (0.3)	2.2E-02 (0.8)	9.8E-02 (0.2)	3.0E-02 (0.7)
Brain	9.1E-02 (1.1)	1.8E-02 (2.7)	1.7E-01 (0.8)	2.5E-02 (2.3)
Salivary glands	3.3E-02 (2.1)	1.3E-02 (3.6)	5.5E-02 (1.6)	1.7E-02 (3.2)
Skin	1.8E-01 (0.2)	2.6E-02 (0.5)	2.5E-01 (0.2)	3.4E-02 (0.5)
Eye lens	8.5E-02 (12)	3.0E-02 (20)	1.7E-01 (9.0)	3.9E-02 (18)
$CC[E]_{Male}$ ($\mu Sv/Gy.cm^2$)	4.7E-02 (2.0)	3.9E-03 (7.0)	8.5E-02 (2.0)	5.4E-03 (5.0)

[a] Adrenals, extratoracic region, gall bladder, kidneys, lymphatic nodes, muscle, oral mucosa, pancreas, prostate, small intestine, spleen, thymus and heart.

Table 5
$CC[H_T]_{Male}$ and $CC[E]_{Male}$ ($\mu Sv/Gy.cm^2$) for the male main and assistant physicians (MASH3): without suspended shield. Type A uncertainties are presented in parentheses (in %).

	Scenario without suspended shield			
	70 kVp		80 kVp	
Male **Organ/ Tissue**	**Main Physician**	**Assistant Physician**	**Main Physician**	**Assistant Physician**
Bone marrow	4.0E-01 (0.1)	1.3E-02 (0.6)	5.2E-01 (0.1)	1.7E-02 (0.5)
Colon	2.4E-01 (0.8)	1.4E-03 (9.0)	3.2E-01 (0.7)	2.5E-03 (7.6)
Lung	7.8E-01 (0.3)	1.2E-02 (2.3)	1.1E+00 (0.2)	1.5E-02 (2.0)
Stomach	1.8E-01 (1.3)	1.5E-03 (17)	2.7E-01 (1.1)	1.5E-03 (16)
Breast	1.0E+00 (1.2)	8.1E-03 (14)	1.2E+00 (1.1)	9.4E-03 (14)
Remainder tissues[a]	5.6E-02 (0.1)	1.2E-03 (0.5)	6.9E-02 (0.1)	1.6E-03 (0.5)
Gonads	2.4E-03 (25)	1.9E-04 (55)	5.8E-03 (19)	2.1E-03 (34)
Bladder	6.4E-03 (9.0)	5.5E-04 (38)	1.3E-02 (7.4)	6.0E-04 (40)
Oesophagus	3.5E-01 (1.5)	7.5E-03 (12)	5.2E-01 (1.2)	1.1E-02 (9.3)
Liver	1.3E+00 (0.3)	4.3E-03 (4.9)	1.7E+00 (0.3)	5.9E-03 (4.4)
Thyroid	1.5E-01 (3.9)	1.2E-02 (15)	2.0E-01 (3.2)	1.4E-02 (12)
Bone surface	4.0E-01 (0.1)	3.4E-02 (0.6)	5.0E-01 (0.1)	4.6E-02 (0.6)
Brain	7.6E-01 (0.4)	3.3E-02 (1.9)	1.1E+00 (0.3)	4.7E-02 (1.7)
Salivary glands	2.8E-01 (0.7)	2.0E-02 (3.0)	3.6E-01 (0.6)	2.5E-02 (2.7)
Skin	1.1E+00 (0.1)	3.9E-02 (0.4)	1.3E+00 (0.1)	5.0E-02 (0.4)
Eye lens	6.1E-01 (5.0)	6.0E-02 (14)	8.2E-01 (4.0)	8.2E-02 (13)
$CC[E]_{Male}$ ($\mu Sv/Gy.cm^2$)	4.1E-01 (2.0)	6.7E-03 (6.0)	5.4E-01 (2.0)	8.8E-03 (4.0)

[a] Adrenals, extratoracic region, gall bladder, kidneys, lymphatic nodes, muscle, oral mucosa, pancreas, prostate, small intestine, spleen, thymus and heart.

voltage and the use or disuse of the CPE, such as the lead curtain, suspended shield and fetal shield, for the male main and assistant physicians (Tables 2–5), and for the female main and assistant physicians (Tables 6–9).

Comparing all scenarios, including those without CPE, and tube voltages, the most irradiated organs/tissues are quasi the same for the main and assistant physicians, independent of the configurations. For the male main physician the organs are brain, liver and skin, as for the female main physician they are the breast, liver, skin (brain is the 4rth most irradiated). To some of these organs, the explanation is straightforward, as for the skin. The skin lacks protection, given that it is virtually impossible to cover all the body with lead. The liver is a large organ, located near the X-ray tube, and the side and rear apertures in the lead apron provides a good evidence for its higher doses. The brain, in our simulations, received no protection and the male breasts are smaller than those from the female physicians.

The comparison for the male and female assistant physician includes, for the male, bone surface, eye lens, skin (brain is the 4rth most irradiated) and, for the female, eye lens, brain, skin. In this case, the liver is protected by the main physician, which absorbs a considerable part of the scattered radiation. Here, the eye lens appears within the three most irradiated organs/tissues, but even for the main physicians they presented high $CC[H_T]$ values. A more detailed description of the $CC[H_T]_{eye\ lens}$ will be presented in section 3.1.

With Equation (1) the CC[E] values ($\mu Sv/Gy.cm^2$) for the main and assistant physicians were determined (uncertainties in % in parentheses), for both tube voltages. For a 70 kVp tube voltage, the values were 5.6E-02 (2.0) for the $CC[E]_{Physician}$ and 4.1E-03 (6.5) for the $CC[E]_{Assistant}$. For an 80 kVp tube voltage the values were 9.9E-02 (1.5) for the $CC[E]_{Physician}$ and 5.6E-03 (5.5) for the $CC[E]_{Assistant}$. The differences between the main and the assistant physicians were higher than 90%, for both tube voltages, showing the influence of the distance from the X-ray source, but also the influence of the shielding offered by the main to the assistant physician. The influence of the tube voltage on the CC[E] values may be observed comparing both main and assistant physicians. The difference between the physicians was 43%, and for the assistants 27%. This influence will be better presented in section 3.1.

As can be seen in Fig. 2, both main and assistant physicians are laterally positioned relative to the patient and, therefore, part of the radiation scattered by the patient, and other structures, passes through the gap between the lead apron and the left arm. The pelvic region organs of both genders, as the bladder, gonads and part of the organs and tissues located in the abdominal region, as adrenal glands, biliary bladder, kidneys, pancreas, small intestine and spleen are protected by the apron and by the lead curtain and, therefore, obtained the lowest $CC[H_T]$ values. Besides of the patient table, the lowest energy photons are attenuated by the patient ribs and/or are absorbed by the large amount of tissues found in the beam path; consequently, when the X-ray equipment is operated with 70 kVp, it represents a less critical situation for the medical staff.

3.1. Effect of tube voltage and the use of suspended shield and lead curtain on the occupational exposure

Using Equations (2) and (3), and the $CC[H_T]$ values presented in Table 2 to Table 9 for the MASH3 and FASH3 phantoms, the $CC[E]_{Male}$ and $CC[E]_{Female}$, for the main and the assistant physicians were obtained, as a function of the tube voltage and the use or disuse of the CPE. The CPE evaluated in this work were the lead curtain, suspended shield and fetal shield.

The CC[E] values for the complete scenario (using all CPE as presented in Fig. 2), without the lead curtain, suspended shield and fetal shield are presented in Table 10. With these analyses it is possible to evaluate the influence of these protective equipment on the individuals. Four different scenarios were considered: complete scenario; absence of lead curtain and suspended shield; absence of the fetal shield; and

Table 6
$CC[H_T]_{Female}$ and $CC[E]_{Female}$ ($\mu Sv/Gy.cm^2$) for the female main and assistant physicians (FASH3): with lead curtain, suspended shield and fetal shield. Type A uncertainties are presented in parentheses (*in* %).

	Scenario with all protective equipment			
	70 kVp		80 kVp	
Female **Organ/Tissue**	**Main Physician**	**Assistant** Physician	**Main** Physician	**Assistant** Physician
Bone marrow	8.6E-02 (0.2)	2.7E-03 (1.3)	1.3E-01 (0.2)	3.8E-03 (1.1)
Colon	8.0E-02 (1.3)	2.4E-03 (7.4)	1.3E-01 (1.0)	3.7E-03 (6.3)
Lung	1.0E-01 (0.8)	1.1E-02 (2.5)	1.9E-01 (0.6)	1.5E-02 (2.2)
Stomach	3.7E-02 (3.1)	1.5E-03 (16)	7.3E-02 (2.2)	2.2E-03 (14)
Breast	1.2E-01 (1.1)	5.7E-03 (5.9)	2.1E-01 (0.9)	8.2E-03 (5.2)
Remainder tissues[a]	5.5E-03 (0.3)	6.8E-04 (0.8)	9.1E-03 (0.2)	9.3E-04 (0.7)
Gonads	8.8E-03 (18)	5.7E-04 (57)	1.4E-02 (13)	1.7E-04 (75)
Bladder	4.5E-03 (15)	2.6E-04 (59)	1.0E-02 (11)	1.6E-03 (30)
Oesophagus	4.9E-02 (3.8)	5.6E-03 (12)	1.1E-01 (2.6)	7.7E-03 (11)
Liver	1.5E-01 (0.9)	5.6E-03 (4.5)	2.9E-01 (0.7)	8.1E-03 (4.0)
Thyroid	2.7E-02 (9.1)	1.5E-02 (13)	5.1E-02 (6.3)	1.5E-02 (13)
Bone surface	8.4E-02 (0.2)	7.8E-03 (1.5)	1.2E-01 (0.2)	1.1E-02 (1.3)
Brain	9.8E-02 (1.1)	1.9E-02 (2.7)	1.8E-01 (0.8)	2.7E-02 (2.4)
Salivary glands	3.6E-02 (2.1)	1.3E-02 (4.0)	6.2E-02 (1.6)	1.6E-02 (3.7)
Skin	1.8E-01 (0.2)	2.4E-02 (0.6)	2.6E-01 (0.2)	3.2E-02 (0.5)
Eye lens	5.4E-02 (13)	1.6E-02 (23)	7.7E-02 (12)	2.5E-02 (19)
$CC[E]_{Female}$ ($\mu Sv/Gy.cm^2$)	6.5E-02 (2.0)	4.6E-03 (6.0)	1.1E-01 (1.0)	6.2E-03 (6.0)

[a] Adrenals, extratoracic region, gall bladder, kidneys, lymphatic nodes, muscle, oral mucosa, pancreas, uterus, small intestine, spleen, thymus and heart.

Table 7
$CC[H_T]_{Female}$ and $CC[E]_{Female}$ ($\mu Sv/Gy.cm^2$) for the female main and assistant physicians (FASH3): without lead curtain and suspended shield. Type A uncertainties are presented in parentheses (in %).

	Scenario without lead curtain and suspended shield			
	70 kVp		80 kVp	
Female Organ/ Tissue	**Main Physician**	**Assistant Physician**	**Main Physician**	**Assistant Physician**
Bone marrow	6.6E-01 (0.1)	7.2E-03 (0.8)	8.3E-01 (0.1)	9.7E-03 (0.7)
Colon	5.1E-01 (0.5)	4.7E-03 (5.2)	6.8E-01 (0.5)	6.8E-03 (4.6)
Lung	1.1E + 00 (0.2)	2.5E-02 (1.7)	1.4E + 00 (0.2)	3.3E-02 (1.5)
Stomach	2.7E-01 (1.1)	4.0E-03 (10)	4.1E-01 (0.9)	5.3E-03 (8.8)
Breast	1.8E + 00 (0.3)	1.9E-02 (3.3)	2.1E + 00 (0.3)	2.4E-02 (3.0)
Remainder tissues[a]	5.9E-02 (0.1)	1.8E-03 (0.5)	7.2E-02 (0.1)	2.3E-03 (0.4)
Gonads	3.9E-02 (8.7)	1.2E-03 (49)	6.9E-02 (6.5)	1.2E-03 (46)
Bladder	2.8E-02 (6.2)	1.3E-03 (27)	4.5E-02 (5.0)	2.8E-03 (22)
Oesophagus	4.3E-01 (1.3)	1.1E-02 (8.6)	6.4E-01 (1.1)	1.5E-02 (8.1)
Liver	1.7E + 00 (0.3)	1.2E-02 (3.2)	2.3E + 00 (0.2)	1.7E-02 (2.8)
Thyroid	1.8E-01 (3.6)	2.6E-02 (10)	2.5E-01 (3.0)	2.5E-02 (10)
Bone surface	6.6E-01 (0.1)	1.9E-02 (1.0)	8.1E-01 (0.1)	2.6E-02 (0.9)
Brain	8.7E-01 (0.4)	4.0E-02 (1.9)	1.2E + 00 (0.3)	5.6E-02 (1.6)
Salivary glands	3.8E-01 (0.6)	2.1E-02 (3.2)	4.8E-01 (0.6)	2.6E-02 (2.9)
Skin	1.9E + 00 (0.1)	7.1E-02 (0.4)	2.2E + 00 (0.1)	9.1E-02 (0.3)
Eye lens	3.0E-01 (6.0)	4.2E-02 (15)	4.1E-01 (5.0)	5.7E-02 (15)
$CC[E]_{Female}$ ($\mu Sv/Gy.cm^2$)	6.6E-01 (1.0)	1.1E-02 (4.0)	8.4E-01 (1.0)	1.4E-02 (4.0)

[a] Adrenals, extratoracic region, gall bladder, kidneys, lymphatic nodes, muscle, oral mucosa, pancreas, uterus, small intestine, spleen, thymus and heart.

Table 8
$CC[H_T]_{Female}$ and $CC[E]_{Female}$ ($\mu Sv/Gy.cm^2$) for the female main and assistant physicians (FASH3): without fetal shield. Type A uncertainties are presented in parentheses (in %).

	Scenario without fetal shield			
	70 kVp		80 kVp	
Female Organ/ Tissue	**Main Physician**	**Assistant Physician**	**Main Physician**	**Assistant Physician**
Bone marrow	8.7E-02 (0.2)	3.0E-03 (1.2)	1.3E-01 (0.2)	4.1E-03 (1.1)
Colon	8.1E-02 (1.3)	2.8E-03 (6.8)	1.3E-01 (1.0)	4.2E-03 (5.9)
Lung	1.0E-01 (0.8)	1.2E-02 (2.3)	1.9E-01 (0.6)	1.7E-02 (2.1)
Stomach	3.7E-02 (3.0)	1.7E-03 (15)	7.4E-02 (2.2)	2.4E-03 (13)
Breast	1.2E-01 (1.1)	6.3E-03 (5.6)	2.1E-01 (0.9)	9.0E-03 (4.9)
Remainder tissues[a]	5.7E-03 (0.3)	7.6E-04 (0.7)	9.3E-03 (0.2)	1.0E-03 (0.7)
Gonads	9.0E-03 (17)	5.7E-04 (57)	1.4E-02 (13)	1.7E-04 (75)
Bladder	4.7E-03 (15)	5.5E-04 (50)	1.0E-02 (11)	1.6E-03 (30)
Oesophagus	5.0E-02 (3.8)	6.1E-03 (12)	1.1E-01 (2.6)	8.4E-03 (10)
Liver	1.5E-01 (0.9)	6.4E-03 (4.2)	2.9E-01 (0.7)	9.0E-03 (3.9)
Thyroid	2.7E-02 (8.9)	1.6E-02 (13)	5.4E-02 (6.2)	1.6E-02 (13)
Bone surface	8.5E-02 (0.2)	8.7E-03 (1.4)	1.2E-01 (0.2)	1.2E-02 (1.2)
Brain	1.0E-01 (1.1)	2.1E-02 (2.6)	1.8E-01 (0.8)	2.9E-02 (2.2)
Salivary glands	3.7E-02 (2.1)	1.4E-02 (3.8)	6.3E-02 (1.5)	1.7E-02 (3.5)
Skin	1.9E-01 (0.2)	2.6E-02 (0.6)	2.7E-01 (0.2)	3.5E-02 (0.5)
Eye lens	5.6E-02 (13)	1.6E-02 (23)	7.7E-02 (12)	2.5E-02 (19)
$CC[E]_{Female}$ ($\mu Sv/Gy.cm^2$)	6.6E-02 (2.0)	5.1E-03 (5.0)	1.2E-01 (1.0)	6.8E-03 (6.0)

[a] Adrenals, extratoracic region, gall bladder, kidneys, lymphatic nodes, muscle, oral mucosa, pancreas, uterus, small intestine, spleen, thymus and heart.

absence of the suspended shield. In all configurations, the medical staff used lead apron, eyewear and thyroid protectors.

The scenario without the lead curtain and suspended shield obtained the highest CC[E] values presenting a difference above 900% compared with the complete scenario. Removing the suspended shield, the difference from the complete scenario, were up to 811%, demonstrating the importance of the suspended shield during ERCP procedures. The evaluation of the fetal shield must be cautious. The CC[E] presented in Table 10 are for the medical staff, and not the patient, or the fetus, and evaluating the arrangement, its influence should be almost null.

Besides the type of protection, the CC[E] have an important spectral influence. It is observed for the same configuration, that as the tube voltage was increased from 70 kVp to 80 kVp, which determines the energy spectra for the photons emitted from the tube, the $CC[H_T]$ of all organs and tissues increased due to the increase in scattering, mainly,

Table 9
$CC[H_T]_{Female}$ and $CC[E]_{Female}$ ($\mu Sv/Gy.cm^2$) for the female main and assistant physicians (FASH3): without suspended shield. Type A uncertainties are presented in parentheses (in %).

	Scenario without suspended shield			
	70 kVp		80 kVp	
Female **Organ/ Tissue**	**Main Physician**	**Assistant Physician**	**Main Physician**	**Assistant Physician**
Bone marrow	4.7E-01 (0.1)	4.5E-03 (1.0)	6.0E-01 (0.1)	6.2E-03 (0.9)
Colon	4.9E-01 (0.5)	4.1E-03 (5.6)	6.6E-01 (0.5)	6.0E-03 (4.9)
Lung	1.0E+00 (0.3)	2.1E-02 (1.8)	1.4E+00 (0.2)	2.8E-02 (1.6)
Stomach	2.7E-01 (1.1)	3.4E-03 (11)	4.0E-01 (0.9)	4.3E-03 (9.8)
Breast	1.7E+00 (0.3)	1.7E-02 (3.4)	2.1E+00 (0.3)	2.2E-02 (3.1)
Remainder tissues[a]	5.1E-02 (0.1)	1.2E-03 (0.6)	6.3E-02 (0.1)	1.5E-03 (0.5)
Gonads	3.7E-02 (8.9)	3.5E-04 (69)	6.7E-02 (6.6)	3.9E-04 (65)
Bladder	2.0E-02 (7.3)	6.0E-04 (42)	3.5E-02 (5.5)	1.7E-03 (29)
Oesophagus	4.3E-01 (1.4)	1.0E-02 (9.0)	6.3E-01 (1.1)	1.3E-02 (8.5)
Liver	1.7E+00 (0.3)	1.0E-02 (3.4)	2.2E+00 (0.2)	1.4E-02 (3.1)
Thyroid	1.8E-01 (3.6)	2.6E-02 (10)	2.5E-01 (3.0)	2.4E-02 (10)
Bone surface	4.6E-01 (0.1)	1.4E-02 (1.1)	5.8E-01 (0.1)	1.9E-02 (1.0)
Brain	8.7E-01 (0.4)	3.8E-02 (1.9)	1.2E+00 (0.3)	5.4E-02 (1.7)
Salivary glands	3.8E-01 (0.6)	2.1E-02 (3.3)	4.8E-01 (0.6)	2.5E-02 (3.0)
Skin	1.3E+00 (0.1)	4.3E-02 (0.5)	1.5E+00 (0.1)	5.4E-02 (0.4)
Eye lens	3.0E-01 (6.0)	3.9E-02 (15)	4.1E-01 (5.0)	5.6E-02 (15)
$CC[E]_{Female}$ ($\mu Sv/Gy.cm^2$)	6.1E-01 (1.0)	9.2E-03 (6.0)	7.9E-01 (1.0)	1.2E-02 (6.0)

[a] Adrenals, extratoracic region, gall bladder, kidneys, lymphatic nodes, muscle, oral mucosa, pancreas, uterus, small intestine, spleen, thymus and heart.

from the patient body. Moreover, the same tube voltage change leads to an inverse relationship between DAP and kVp. These results are in agreement with the literature (Santos et al., 2018).

Considering a DAP of 7.128 $Gy.cm^2$ (Huda et al., 2015) measured with a X-ray equipment operating at 70 kVp, and using the CC[E] of 5.6E-02 $Sv/Gy.cm^2$ (main physician) and 4.1E-03 $\mu Sv/Gy.cm^2$ (assistant physician), which were obtained in the complete scenario (with the use of lead curtain, suspended shield and fetal shield), representing the safer situation, an effective dose per procedure is obtained for the main and assistant physicians equal to 0.4 μSv and 0.03 μSv, respectively, which are consistent with the results of Sulieman et al. (2011). Considering a workload of 400 ERCP procedures performed by year (Zagorska et al., 2015), the main and assistant physicians received an effective dose of 0.16 mSv/year and 0.01 mSv/year, respectively.

Even though the absence of lead curtain and suspended shield does not surpass the Occupational Exposure limit recommendation from ICRP 103, 2007 (which is also legally established in many countries), the three key principles of radiological protection must be followed. With this in mind, any ECRP procedure room must have all necessary CPE to the medical staff.

On Table 11 the $CC[H_T]_{eye\ lens}$ for the main and assistant physicians, of both genders are presented. The absence of lead curtain and suspended shield were considered the most critical, and corroborate the importance of their use. When they are not used, an increase of 633% in the main physician eye lens may be reached. As an important remark, the use of suspended shield also presented a remarkable reduction in the $CC[H_T]_{brain}$ exposure up to 85% for all situations.

Considering the workload, the DAP previously described, and the results without lead curtain and suspended shield, which were the most critical scenario, the annual equivalent doses of the main physician eye lens was 2.3 mSv/year, and 0.24 mSv/year for the assistant (80 kVp). Considering the scenario with lead curtain and suspended shield these values are reduced to 0.5 mSv/year and 0.1 mSv/year. These results reinforce the importance of keeping all medical staff, involved in ERCP procedures, well informed about the probability of eye lens opacity. They should be trained to correctly use the available suspended shields, in order to minimize the associated radiation risks.

As a consequence of the position of the assistant physician, the CC values were lower than those from the main physician. This may be viewed in Fig. 3, which represents the particle flux distribution calculated inside the room. This was carried out at the abdominal level of the medical staff, with the *mesh tally* plot from MCNPX code, and using a tube voltage of 80 kVp. As can be seen, in the patient surroundings the particle flux is much more intense. The lead curtain and suspended shield importance, on the occupational exposures, may be visualized comparing Fig. 3 left side (Fig. 3 (A) and (C)) to its right side (Fig. 3 (B) and (D)).

Generally, the ERCP procedures demand a fairly close proximity between the medical staff and the patient, justifying the use of all available CPE in order to reduce the radiation exposures. The use of the smallest FOV possible is another way to reduce the scattered radiation level, as showed in a previous study (Santos et al., 2018).

3.2. $CC[H_T]$ and CC[E] for patient and fetus

In the photon energy range evaluated in this study, the $CC[H_T]$ values increased with the tube voltage increment, as can be observed in Table 12. Moreover, the X-ray tube position relative to the patient table also affects the results. Its materials attenuate part of the low energy photons that would be deposited in the patient and fetus. However, is it important to emphasize that during clinical practice, when the examined region thickness is increased, the X-ray equipment triggers the automatic exposure control (AEC) to maintain the image quality. Although this parameter was not evaluated in this study, the change from 70 kVp to 80 kVp might be a good approximation to AEC use, which will compensate for table attenuation. In addition to the tube voltage, the organ location relative to the X-ray beam also leads to patient

Table 10
CC[E] ($\mu Sv/Gy.cm^2$) for occupational exposures, as a function of tube voltage and CPE. The complete scenario is presented in Fig. 2, and comprises a scenario with lead curtain, suspended shield and fetal shield. Each removed CPE is described in the first column. The uncertainties are presented in parentheses (in %).

	70 kVp		80 kVp	
Configuration	Main Physician	Assistant Physician	Main Physician	Assistant Physician
Complete scenario	5.6E-02 (2.0)	4.1E-03 (6.5)	9.9E-02 (1.5)	5.6E-03 (5.5)
Without lead curtain and suspended shield	5.6E-01 (1.0)	1.0E-02 (3.5)	7.2E-01 (1.0)	1.4E-02 (3.5)
Difference (%)	900 %	144 %	627 %	150 %
Without suspended shield	5.1E-01 (1.5)	7.9E-03 (6.0)	6.6E-01 (1.5)	1.0E-02 (5.0)
Difference (%)	811 %	93 %	567 %	79 %
Without fetal shield	5.7E-02 (2.0)	4.5E-03 (6.0)	1.0E-01 (1.5)	6.1E-03 (5.5)
Difference (%)	2 %	10 %	1 %	9 %

Table 11
$CC[H_T]_{eye\ lens}$ ($\mu Sv/Gy.cm^2$) calculated for the Male and Female main and assistant physicians, as a function of tube voltage, and use or not of protective equipment. The complete scenario is presented in Fig. 2, and comprises a scenario with lead curtain, suspended shield and fetal shield (their presence is described in the column configuration). The uncertainties are presented in parentheses (%).

	70 kVp		80 kVp	
	Main	Assistant	Main	Assistant
Configuration	**Male Physicians**			
Complete scenario	8.4E-02 (12)	3.0E-02 (20)	1.7E-01 (9)	3.9E-02 (18)
Without lead curtain and suspended shield	6.2E-01 (5)	6.1E-02 (14)	8.2E-01 (4)	8.4E-02 (12)
Difference (%)	633%	107%	392%	116%
Without fetal shield	8.5E-02 (12)	3.0E-02 (20)	1.7E-01 (9)	3.9E-02 (18)
Difference (%)	1%	0	0	0
Without suspended shield	6.1E-01 (5)	6.0E-02 (14)	8.2E-01 (4)	8.2E-02 (13)
Difference (%)	628%	103%	392%	113%
	Female Physicians			
Complete scenario	5.4E-02 (13)	1.6E-02 (23)	7.7E-02 (12)	2.5E-02 (19)
Without lead curtain and suspended shield	3.0E-01 (6)	4.2E-02 (15)	4.1E-01 (5)	5.7E-02 (15)
Difference (%)	461%	154%	431%	125%
Without fetal shield	5.6E-02 (13)	1.6E-02 (23)	7.7E-02 (12)	2.5E-02 (19)
Difference (%)	4%	0	0	0
Without suspended shield	3.0E-01 (6)	3.9E-02 (15)	4.1E-01 (5)	5.6E-02 (15)
Difference (%)	459%	136%	431%	122%

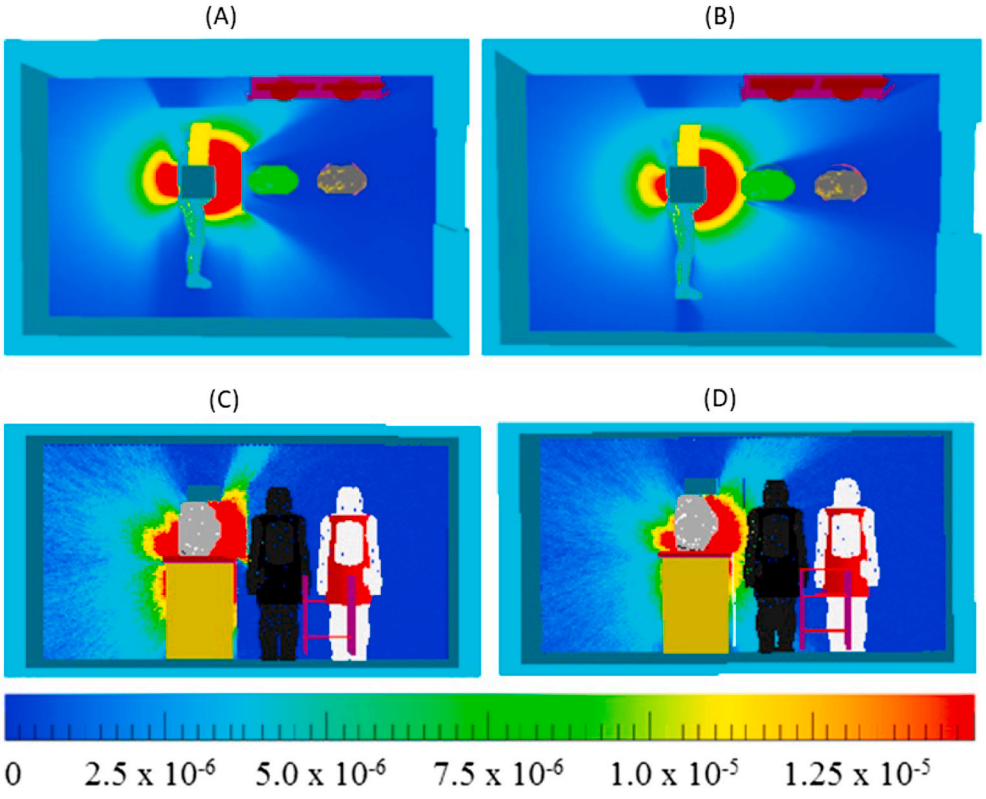

Fig. 3. Two dimensional photon flux distribution views (in MeV/cm^2/particle) inside the room. These maps were obtained at 130 cm above the floor, at the main and assistant physicians abdominal level (A and B), and in front of the physicians (C and D). Each map was calculated for two configurations, with lead curtain and suspended shield (A and C), and without them (B and D).

$CC[H_T]$ value changes. Organs located close, or within, the field of view (FOV) (colon, stomach, liver) and fetus were the most exposed, compared with organs distant or distributed all over the body (red bone marrow, remainder tissues, gonads, bladder, thyroid, bone surface, brain, salivary glands, skin and eyes). The FOV increase does not lead to large changes in the patient CC[E] values, as presented in the study of Santos et al. (2018).

As can be seen in Table 12, colon, lung, stomach and breasts presented high $CC[H_T]$ values. These organs have some of the highest tissue weighting factors (w_T = 0.12) and this resulted in higher CC[E] values.

Even though there is no effective dose limit to medical exposure, in this study, it was decided to present them, believing that it is important to provide values to be compared among services of the same medical institution or different institutions. A second factor is that there are few dosimetric data of pregnant patients and, therefore, the $CC[E]_{Patient}$ presentation may be a valuable source of information. The minimum and maximum $CC[E]_{Patient}$ values in (mSv/Gy.cm^2) were 1.3E-01 (70 kVp) and 1.5E-01 (80 kVp). These results are in agreement with the experimental results described in the literature (1.5E-01 mSv/Gy.cm^2) (Samara et al., 2009).

The absorbed doses in the fetus may vary among different ERCP procedures. The ICRP 103, 2007 recommends that when the dosimetric values exceed the 100 mGy threshold, it is necessary to inform the mother about the dosimetric values, and the related childhood cancer risks. Considering a DAP of 7.128 Gy.cm^2 (Huda et al., 2015), the

Table 12
CC[H_T] and CC[E] (mSv/Gy.cm^2) for MARIA (patient). The complete scenario is presented in Fig. 2, and comprises a scenario with lead curtain, suspended shield and fetal shield. The Type A uncertainties are presented in parentheses (*in %*).

	70 kVp		80 kVp	
Patient Organ/ Tissue	Complete scenario	Without fetal shield	Complete scenario	Without fetal shield
Bone marrow	4.1E-03 (0.1)	4.1E-03 (0.1)	5.0E-03 (0.1)	5.0E-03 (0.1)
Colon	2.4E-01 (0.1)	2.4E-01 (0.1)	2.9E-01 (0.1)	2.9E-01 (0.1)
Lung	1.6E-01 (0.1)	1.6E-01 (0.1)	1.9E-01 (0.1)	1.9E-01 (0.1)
Stomach	2.1E-01 (0.1)	2.1E-01 (0.1)	2.7E-01 (0.1)	2.7E-01 (0.1)
Breast	1.1E-01 (0.1)	1.1E-01 (0.1)	1.3E-01 (0.1)	1.3E-01 (0.1)
Remainder tissues[a]	5.5E-03 (0.1)	5.5E-03 (0.1)	6.3E-03 (0.1)	6.3E-03 (0.1)
Gonads	3.0E-03 (1.1)	3.0E-03 (1.1)	4.5E-03 (0.9)	4.5E-03 (0.9)
Bladder	4.6E-03 (0.7)	4.6E-03 (0.7)	6.9E-03 (0.6)	6.9E-03 (0.6)
Oesophagus	1.5E-01 (0.1)	1.5E-01 (0.1)	1.9E-01 (0.1)	1.9E-01 (0.1)
Liver	7.8E-01 (0.1)	7.8E-01 (0.1)	9.2E-01 (0.1)	9.2E-01 (0.1)
Thyroid	3.8E-03 (1.3)	3.9E-03 (1.2)	5.4E-03 (1.1)	5.5E-03 (1.0)
Bone surface	4.1E-03 (0.1)	4.1E-03 (0.1)	5.0E-03 (0.1)	5.0E-03 (0.4)
Brain	6.4E-04 (0.5)	6.5E-04 (0.5)	8.9E-04 (0.4)	9.0E-04 (0.3)
Salivary glands	2.9E-03 (0.3)	2.9E-03 (0.3)	3.3E-03 (0.3)	3.3E-03 (0.1)
Skin	8.0E-02 (0.1)	8.0E-02 (0.1)	8.7E-02 (0.1)	8.7E-02 (0.8)
Eyes	5.1E-04 (0.8)	5.2E-04 (0.8)	6.3E-04 (0.8)	6.3E-04 (0.1)
Fetal dose	2.2E-01 (0.1)	2.2E-01 (0.1)	2.6E-01 (0.1)	2.7E-01 (0.1)
ESD	3.0E+00 (0.1)	3.0E+00 (0.1)	3.0E+00 (0.1)	3.0E+00 (0.1)
$CC[E]_{Patient}$ (mSv/ Gy.cm^2)	1.3E-01 (0.1)	1.3E-01 (0.1)	1.5E-01 (0.1)	1.5E-01 (0.1)

[a] Adrenals, extratoracic region, gall bladder, kidneys, lymphatic nodes, muscle, oral mucosa, pancreas, uterus, small intestine, spleen, thymus and heart.

patient and the fetus effective doses were 0.9 mSv and 1.1 mSv (70 kVp) and 1.6 mGy and 2 mGy (80 kVp). In this scenario, the fetal shield did not affect the results. In these simulations, the FOV was not positioned over the fetal shield, which means that the fetal dose was solely by the scattered radiation inside the patient body. However, care must be taken before any further conclusion. In some situations, the primary radiation beam may, accidently and inadvertently, expose the fetus (e.g. table movement or X-ray tube positioning). In this case, the fetal shield will protect the fetus from this unwanted exposition to the primary beam.

Once more, to compare our results with experimental data, from the literature, a DAP of 7.128 Gy.cm^2 (Huda et al., 2015) was considered. In the work of Huda et al. (2015) different patient's organs were evaluated, and a complete comparison is not possible, but an estimation of the patient effective dose ($E_{Patient}$) may be carried out when the same organs are compared. The values obtained were 0.63 mSv in the work of Huda et al. (2015) and 0.68 mSv in this work, which represents a 7% difference.

The fetal dose presented a difference of 94% from Huda et al. (2015). Part of this difference may be attributed to the gestational stage. In this work the patient is in the second trimester, while Huda et al. (2015) used a phantom representing a 9-month pregnant patient. However, comparing to experimental measurements, the result in this work is within the range found in the work of Kahaleh et al. (2004), who obtained mean fetal absorbed doses between 0.01 and 1.8 mGy (in this work the fetal dose was 1.6 mGy). The study was conducted with 17 pregnant women, with an average gestational age of 18.6 weeks, and an interval of 6–33 weeks.

Using the fetus absorbed dose and the cancer induction coefficient of 5.5E-02/Gy (in Equation (6)) the minimum and maximum cancer induction values of 8.2E-05 and 1.1E-04 were obtained. These values are comparable with the literature (1.0E-04) (Samara et al., 2009). The small differences may be attributed to the virtual anthropomorphic phantoms models involved in this study (voxel based phantoms) and the one used by Samara et al. (2009), which was a stylized phantom. In this case, the organs and tissues are represented by mathematical equations, which limit a more realistic representation of distances between organs compared with voxel phantoms.

Is this study, the simulations were performed with 1E9 photon histories to assure statistical uncertainties within acceptable limits. However, even for such a large photon histories number, the gonads and bladder of the medical staff, which are located more internally and are, naturally more protected, presented uncertainties above 50%, when the reference configuration was used. The organs with large volumes (liver, lung, colon, stomach, etc) or relatively uniformly distributed throughout the whole body (skin, bone surface, red bone marrow, etc) obtained lower uncertainties, compared with organs with lower volumes like the thyroid and the eye lens. For the patient, the results for all CC values presented low uncertainties. With exception to the gonads and the thyroid, which presented uncertainties between 1 and 2%, the majority of the structures reached uncertainties below 0.5%.

4. Conclusions

The results clearly show the importance of the lead curtain and suspended shield. These CPE, with 0.5 mmPb equivalent thickness, when not used may increase the CC[E] between 627% to 900% to the main physician and of 140%–150% to the assistant physician. It is important to highlight that the CC[E] reduction, among other factors, depends on the applied X-ray tube voltage. When the lead curtain is used, but the suspended shield is neglected, the main and assistant physicians $CC[H_T]_{eye\ lens}$ values increased to 460%–628% for the main physicians and 100%–136% for the assistant physicians. These results highlight the importance, and proper, use of all available CPE. The maximum fetus absorbed dose represents approximately 2% of the value regarded as the induced risk (> 100 mGy), but the FOV was not directed to the fetus. The fetal shield also presented no influence in this configuration, but when the FOV was directed to the fetus, the absorbed dose reduction was 97% with this protective device. Considering that during ERCP procedures the irradiated region may change, the fetal shield is an indispensable device.

CRediT authorship contribution statement

William S. Santos: Conceptualization, Methodology, Visualization, Investigation, Writing - original draft, Project administration. **Lucas W.G. Souza:** Software, Investigation, Writing - original draft, Writing - review & editing. **Lucio P. Neves:** Formal analysis, Investigation, Data curation, Funding acquisition, Writing - original draft, Writing - review & editing, Funding acquisition. **Ana P. Perini:** Formal analysis, Investigation, Resources, Writing - original draft, Writing - review & editing, Funding acquisition. **Carla J. Santos:** Software. **Walmir Belinato:** Validation. **Linda V.E. Caldas:** Supervision, Writing - review & editing, Funding acquisition.

Declaration of competing interest

The authors declare that they have no known competing financial interests or personal relationships that could have appeared to influence the work reported in this paper.

Acknowledgements

The authors would like to thank Dr. Richard Kramer for kindly providing the virtual anthropomorphic phantoms. This work was partially supported by the Brazilian agencies FAPEMIG (Grants Nos. APQ-03049-15 and APQ-02934-15), and CNPq (Grants Nos. 421603/2016–0, 420699/2016–3 and 301335/2016–8). L.W.G. Souza received

a Fellowship from FAPEMIG.

References

Al-Hashem, H., Muralidharan, V., Cohen, H., Jamidar, P.A., 2009. Biliary disease in pregnancy with an emphasis on the role of ercp. J. Clin. Gastroenterol. 43, 58–62.

Brenner, D., Huda, W., 2008. Effective dose: a useful concept in diagnostic radiology? Radiat. Protect. Dosim. 128, 503–508.

Cabral, M.O.M., Vieira, J.W., Neto, V.L., de Andrade Lima, F.R., 2015. Development of a pregnant woman phantom using polygonal mesh, for dosimetric evaluations. Brazilian Journal of Radiation Sciences 3.

Cassola, V.F., Lima, V.J.D., Kramer, R., Khoury, H.J., 2010. FASH and MASH: female and male adult human phantoms based on polygon mesh surfaces: I. development of the anatomy. Phys. Med. Biol. 55, 133–162.

Cranley, K., Gilmore, B., Fogarty, G., Despond, L., 1997. Catalogue of diagnostic X-ray data and other data. Tech. Rep. 78 Institute of Physics and Engineering in Medicine (IPEM).

Huda, A., Garzón, W., Filho, G., Vieira, B., Kramer, R., Xu, X., Gao, Y., Khoury, H., 2015. Evaluation of staff, patient and foetal radiation doses due to endoscopic retrograde cholangiopancreatography (ercp) procedures in a pregnant patient. Radiat. Protect. Dosim. 168, 401–407.

ICRP 103, 2007. The 2007 recommendations of the international commission on radiological protection. Ann. For. 37 (2–4).

ICRP 116, 2010. Conversion coefficients for radiological protection quantities for external radiation exposures. Ann. ICRP 40 (2–5).

ICRP 89, 2002. Basic anatomical and physiological data for use in radiological protection reference values. Ann. ICRP 32 (3–4).

Kahaleh, M., Hartwell, G.D., Arseneau, K.O., Pajewski, T.N., Mullick, T., Isin, G., Agarwal, S., Yeaton, P., 2004. Safety and efficacy of ercp in pregnancy. Gastrointest. Endosc. 60, 287–292.

Kramer, R., Cassola, V., Khoury, H., Vieira, J., de Melo Lima, V., Brown, K.R., 2009. Fash and mash: female and male adult human phantoms based on polygon mesh surfaces: ii. dosimetric calculations. Phys. Med. Biol. 55, 163.

Lee, C., Park, B., Lee, S.-S., Kim, J.-E., Han, S.-S., Huh, K.-H., Yi, W.-J., Heo, M.-S., Choi, S.-C., 2019. Efficacy of the Monte Carlo method and dose reduction strategies in paediatric panoramic radiography. Sci. Rep. 9, 1–10.

Pelowitz, D.B., 2011. MCNPX User's Manual. Los Alamos National Laboratory Version 2.7.0. Report LA-CP-11-00438.

Samara, E.T., Stratakis, J., Melono, J.M.E., Mouzas, I.A., Perisinakis, K., Damilakis, J., 2009. Therapeutic ercp and pregnancy: is the radiation risk for the conceptus trivial? Gastrointest. Endosc. 69, 824–831.

Santos, W.S., Belinato, W., Perini, A.P., Caldas, L.V., Galeano, D.C., Santos, C.J., Neves, L.P., 2018. Occupational exposures during abdominal fluoroscopically guided interventional procedures for different patient sizes a Monte Carlo approach. Phys. Med. 45, 35–43.

Sulieman, A., Paroutoglou, G., Kapsoritakis, A., Kapatenakis, A., Potamianos, S., Vlychou, M., Theodorou, K., 2011. Reduction of radiation doses to patients and staff during endoscopic retrograde cholangiopancreatography. Saudi J. Gastroenterol.: official journal of the Saudi Gastroenterology Association 17, 23.

Tham, T., Vandervoort, J., Wong, R., Montes, H., Roston, A., Slivka, A., Ferrari Jr., A., Lichtenstein, D., Van Dam, J., Nawfel, R., et al., 2003. Safety of ercp during pregnancy. Am. J. Gastroenterol. 98, 308.

Wu, W., Faigel, D.O., Sun, G., Yang, Y., 2014. Non-radiation endoscopic retrograde cholangiopancreatography in the management of choledocholithiasis during pregnancy. Dig. Endosc. 26, 691–700.

Xu, X.G., 2014. An exponential growth of computational phantom research in radiation protection, imaging, and radiotherapy: a review of the fifty-year history. Phys. Med. Biol. 59, R233–302.

Zagorska, A., Romanova, K., Hristova-Popova, J., Vassileva, J., Katzarov, K., 2015. Eye lens exposure to medical staff during endoscopic retrograde cholangiopancreatography. Phys. Med. 31, 781–784.